CONTRIBUTION TO THE STUDY OF TOUGHNESS IN CREEP RESISTANT STEEL WELDED JOINT

E.A.S. Ahmed [a], T. Vuherer [b], V. Grabulov [c], D. Glišić [a], S. Dikić [a,*], N. Radović [a]

[a] University of Belgrade, Faculty of Technology and Metallurgy, Department of Metallurgical Engineering, Belgrade, Serbia
[b] University of Maribor, Faculty of Mechanical Engineering, Maribor, Slovenia
[c] Institute for Materials Testing, Belgrade, Serbia
e-mail: esmail682005@yahoo.com, tomaz.vuherer@um.si, vencislav.grabulov@institutims.rs, gile@tmf.bg.ac.rs, sdikic@tmf.bg.ac.rs, nenrad@tmf.bg.ac.rs

(Received 14 November 2024; Accepted 01 June 2025)

ABSTRACT

Steel P91 is widely used in power stations due to its good creep resistance and predicable performance. The aim of this work was to compare toughness values from different zones in weld joint with sample that underwent simulated thermal cycle. Workpieces were welded using Gas Tungsten Arc Welding (GTAW) for root pass and Manual Metal Arc (MMA) for a filler deposition. Post Welding Heat Treatment (PWHT) was performed on 740°C for 2 hours. Welded joint was tested by means of microstructure, macrostructure, hardness, strength and toughness.
Macrostructure revealed all typical zones, with tempered martensite microstructure. Difference in carbide distribution, confirmed by hardness measurements, occurs as consequence of variations in chemical composition. Tensile strength and fracture which occurred in base metal, indicate good properties of weld joint.
Obtained crack initiation energies were similar across Base Metal (BM), Heat Affected Zone (HAZ), and Weld Metal (WM), while crack propagation energy was lowest in the WM. This indicates that carbides control crack initiation energy, while their distribution influences crack propagation.
Simulated HAZ samples showed lower toughness compared to weld samples due to difference in performed thermal cycles. During welding HAZ undergoes several thermal cycles in each pass, providing smaller austenitic grains compared to simulated HAZ. Lower values of toughness indicate that simulation provides conservative approach, i.e. measured toughness is lower than toughness in real welded butt.

Keyword
Welding, heat affected zone, toughness, post welding heat treatment

INTRODUCTION

Steel X20CrMoV12-1 was introduced approximately 60 years ago in Germany, as first ferritic/martensitic 9-12 % Cr steel for power plants, i.e. turbine components produced by forging [1]. Steel was modified into grade P91 (9%Cr; 1%Mo with V) in order to enhance manufacturing of pipes and vessels [2]. Main properties favoring application of P91 steel are high thermal conductivity and good steam corrosion resistance [3][4][5][6], together with good weldability and microstructural stability [5,7–10], as well as low thermal expansion, good ductility, and high toughness [3,6,9–12].

Most important alloying element in ferritic/martensitic steels is Cr. Cr stabilizes ferritic microstructure and strengthen it by presence in solid solution. Improved high temperature behavior is, due to high Cr affinity towards carbon, provided by presence of carbides, mainly Cr-rich $M_{23}C_6$ type precipitates which pins dislocations and/or subgrain boundaries [5,13–15]. Other common roles of chromium like improved wear resistance, hardenability and even corrosion resistance in high concentrations are welcomed [5,9,14–17]. On the other hand, increase of Cr content can lead to decrease in toughness, having in mind that more than 13% stabilizes delta ferrite and more than 10.5% Cr in solid solution provides stainless behavior [16]. Role of molybdenum is to provide better hardenability as well as prevention of grain boundary glides [15,18]. Due to high affinity to carbon, addition of vanadium provides easy formation of very fine carbides. These carbides consume vacancies and enables particle strengthening improving creep strength [10,14,15,17,19]. P91 steel get its final microstructure after heat treatment. Microstructure consists of tempered martensite with very fine dispersed Cr rich carbides [5,9,14,15,20,21]. During exploitation, martensite plates are dissolving, enabling growth of Cr rich carbides (dominantly $M_{23}C_6$) and formation of V rich carbides [14,20,21].

Steel P91 can be welded by any of the commonly used arc welding processes such as shielded metal arc welding (SMAW), gas tungsten arc welding (GTAW) and submerged arc welding (SAW). In multipass welding, for filling passes Manual Metal Arc (MMA) welding can also be used. The creep strength and other mechanical properties of P91 as base metal (BM) are influenced by the welding process and post welding heat-treatment [5,9,14,17,20,21].

After welding is necessary to make Post Welding Heat Treatment (PWHT), in order to improve toughness and reduce hardness in both weld metal (WM) and Heat Affected Zone (HAZ) [5,9,14–17]. Different PWHT routes are reported, including even air cooling from high temperatures [14,22,23].

Microstructure after PWHT of P91 steel should be as similar to base metal as possible. Therefore, it is expected that tempered martensite with carbide precipitates along grain boundaries [5,13–15,17,24,25] should be dominant. It is reported that temper martensite grain structures of in HAZ are even finer than those of base metal. Also, small differences may lead to difference in toughness, because toughness is very susceptible to changes in size/shape of second phase particles.

Therefore, the aim of this work was to weld P91 steel and to compare toughness measured in different zones in weld joint with samples that underwent simulated/repeated temperature cycle in HAZ.

Experimental part

Chemical composition of tested Cr-Mo type P91 steel is given in Table 1. Steel is characterized with yield stress of min 450MPa and guaranteed impact energy of 41J at room temperature.

Table 1. Chemical composition of tested Cr-Mo type P 91steel

	Chemical composition, mas. %										
	C	Si	Mn	P	S	Cr	Mo	Ni	V	Nb	Cu
Base metal	0.129	0.277	0.443	0.001	0.001	8.25	0.874	0.01	0.198	0.056	0.068
Filler metal	0.11	0.3	0.5			9	0.9	0.5	0.2	0.55	

Experimental welding. Experimental welding was performed on workpieces of plate thickness of 15 mm, length of 500 mm and width of 150mm.

Due to requirement for high quality of welded joints (level ''B'' according to SRPS ISO 5817) a decision was to make root passes (1-4) using TIG (141 according to SRPS EN ISO 4063), double-sided with two passes for each side.

As filler material a bar designated as W CrMo91 according to EN ISO 21952-A was selected (Boehler C 9 MV – IG). Chemical composition of filler material is given in Table 1.

Workpieces were weld using direct current with nonconsumable tungsten electrode with diameter 2.4mm, negative polarity on electrode. Flow of protective gas (Ar) was 12 l/min. Filler deposition, in accordance to scheme was performed using MMA process with coated electrode 3,25mm in diameter, designated as E CrMo91 B 4 2 H5 po EN ISO 3580-a (Boehler FOX C 9 MV)

Welding parameters were selected in accordance with previous practical experience of authors in welding of creep resistant steels [26], and are given in Table 2.

Heat input, Q was calculated separately for each welding pass using Eq.(1).

$$Q = \frac{I \cdot U}{v}, kJ/cm \quad (1)$$

Where: I – Electrical current (A), U – welding voltage(V) and v –welding speed (cm/s).

Table 2. Welding parameters

Pass	Welding Process (EN ISO 4063)	El.Current of welding /A	Voltage of welding /V	Welding speed /cm/s	Heat input /KJ/cm
Root pass	141 - GTAW	172	12,2	0,1	21
Filling passes	111-MMA	126	25,4	0,287	11,2

Two root passes were deposited on each side of symmetrical X groove. Order of deposition was as follows:

- Root pass: GTAW, wire, diameter 2,4mm
- Filling passes: - MMA, electrodes diameter 2,5mm and 3,2mm

Heat treatment. Initial preheating temperature was 250°C, while interpass temperature was maintained in interval 200°C 300°C. Heat cycles were monitored during welding. Sketch of post weld heat treatment is shown in Figure 1. All specimens underwent the same heat treatment that included post weld heat treatment at 740°C for 2 hours [26]. Heating rate was 150°C/s. Between 740 and 200°C specimens were cooled with controlled cooling rate of 150°C/s. Below 200°C specimens were cooled with furnace.

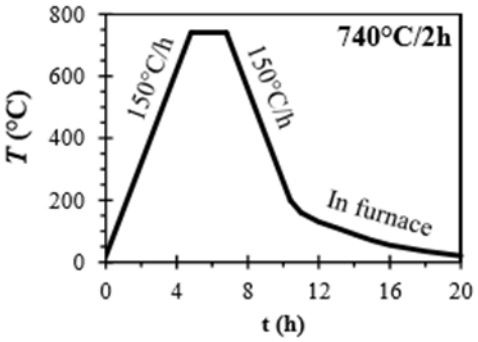

Figure 1. Post Welding Heat Treatment

Simulation. In order to provide sample with microstructure as much as similar to microstructure in HAZ, simulation of thermal cycle monitored in HAZ was reproduced on full size Charpy specimen using Gleeble Welding Simulator. It is necessary to monitor/register the thermal cycle of HAZ (alternatively this thermal cycle can be calculated based on $t_{8/5}$), and to reproduce it on full size Charpy specimen. Sample was heated using electrical resistant heater, coupled with Ni-NiCr thermocouple for control of temperature. After reaching designed temperature and controlled cooling, required microstructure is present in central part of specimen, where notch is going to be placed. In order to provide largest grain size (coarse grained HAZ microstructure), sample was heated up to 1300°C. After cooling, specimen underwent the same heat treatment.

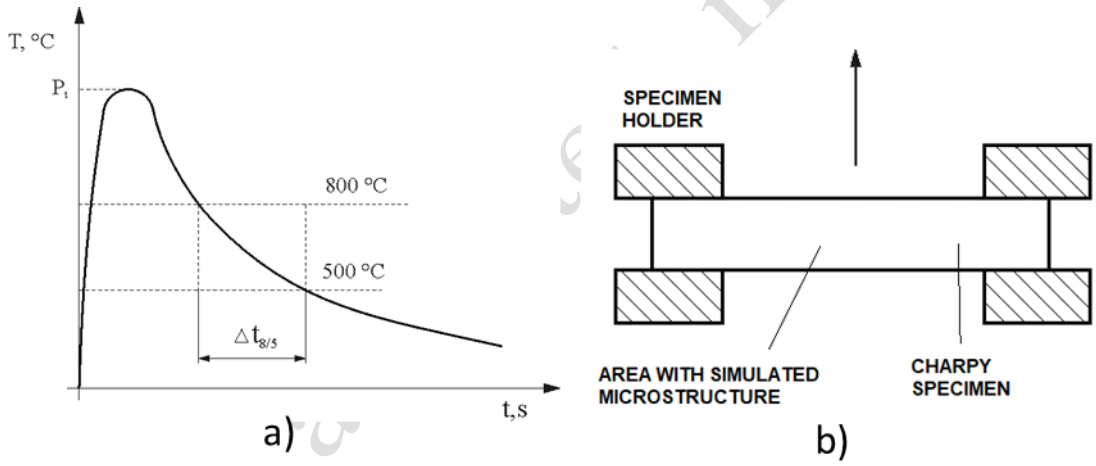

Figure 2. Scheme of simulation: (a) Thermal cycle in HAZ; (b) sample position

Testing of weldment. Mechanical and technological testing were performed in order to establish mechanical properties of both base metal and weld joints: strength, hardness, elasticity, plasticity and absorbed impact energy. Specimens were taken from welded plates in accordance with relevant European standards. Welded plates are shown in Figure 3.

Macro and microstructural characterization of weld joint was conducted according to standard SRPS EN ISO 17639:2014 " Destructive tests on welds in metallic materials. Macroscopic and microscopic examination of welds".

Mechanical and technological testing of welds. Mechanical and technological testing of welds of steel SA 387 Gr. 91 included:

Hardness testing of welds was performed according to standard SRPS EN ISO 9015:2013 "Destructive tests on welds in metallic materials -- Hardness testing -- Part 1: Hardness testing of arc welded joints". Vickers hardness with 100N (HV10) and indentation magnification 100x were used. Hardness was measured on line in different zones (Base metal – HAZ – Weld metal – HAZ – Base metal).

Tensile testing of weldments, with definition of the sizes of test specimen and the procedure for carrying out transverse tensile tests in order to determine the tensile strength and the location of fracture of a welded butt joints, SRPS EN ISO 4136:2013 " Destructive tests on welds in metallic materials -- Transverse tensile test" was used. Testing was carried out at electromechanical tensile testing machine in load control regime. Loading rate was 5 mm/min.
Bending testing was performed according to standard SRPS EN ISO 5173:2013 “Destructive tests on welds in metallic materials -- Bend tests". Specimen dimensions were 300x30x15 mm. Samples were bended over bend former (diameter 4t) with angle of 180. Testing was performed using mechanical tensile machine with controlled displacement. Requirement is that NO cracks longer than 3mm are allowed in any direction.
Toughness. In order to distinguish crack initiation and propagation energies, an instrumented Charpy pendulum was used according to standard SRPS EN ISO 14556:2020 Metallic materials - Charpy V-notch pendulum impact test - Instrumented test method [27].

RESULTS

Welded plates are shown in Figure 3, while macrostructure of weld is shown in Figure 4. All typical zones, base metal, HAZ and weld metal are clearly identified.

Plate 1 Plate 2

Figure 3. Welded joints

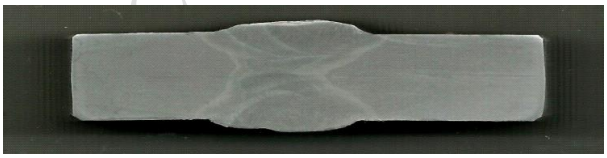

Figure 4. Macrostructure of welded joint

Microstructure analysis. Typical microstructures of BM; HAZ and WM are shown in Figure 5. Since weld joints were exposed to post-welding heat treatment, dominant microstructure in all zones is tempered martensite with some carbides. Small difference is registered in weld metal, due to different chemical composition of filler metal in comparison to base metal heat affected zone.

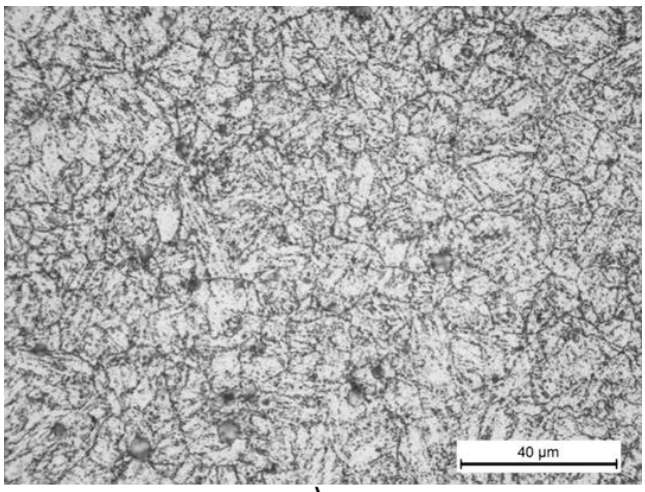

a)

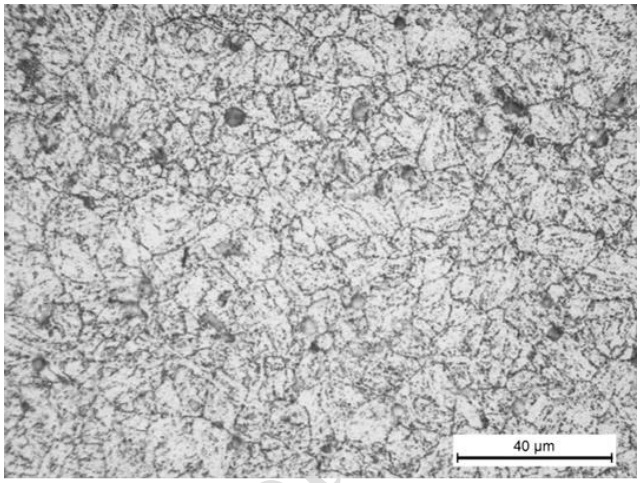

b)

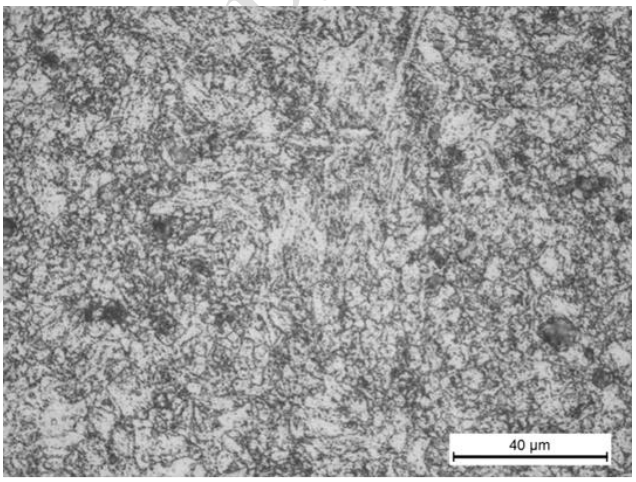

c)

Figure 5. Microstructure in weld joint:
a) BM, b) HAZ, c) WM

Microstructure of base metal, Figure 5a, shows that BM consists of tempered martensite and carbides. Grains are homogenous in shape and size. Carbides are distributed on both grain boundaries and inside grains.

The microstructure of Weld Metal, Figure 5c, looks slightly different because of small difference in chemical composition of filler metal which increased nickel content in weld metal. Distribution of grains is homogeneous with fine carbides inside the grains and on the grain boundaries, Figure 5c. This is

typical tempered martensite. The HAZ has homogenous microstructure which consists of tempered martensite with fine carbides inside and on grain boundary, Figure 5b.
Comparing the grain size of WM and BM, coarser microstructure might be observed in the BM than WM, due to difference in chemical composition of filler metal and higher temperature exposed.
In some areas, coarse grained microstructure is observed, both in BM and HAZ, as shown in Figure 6.

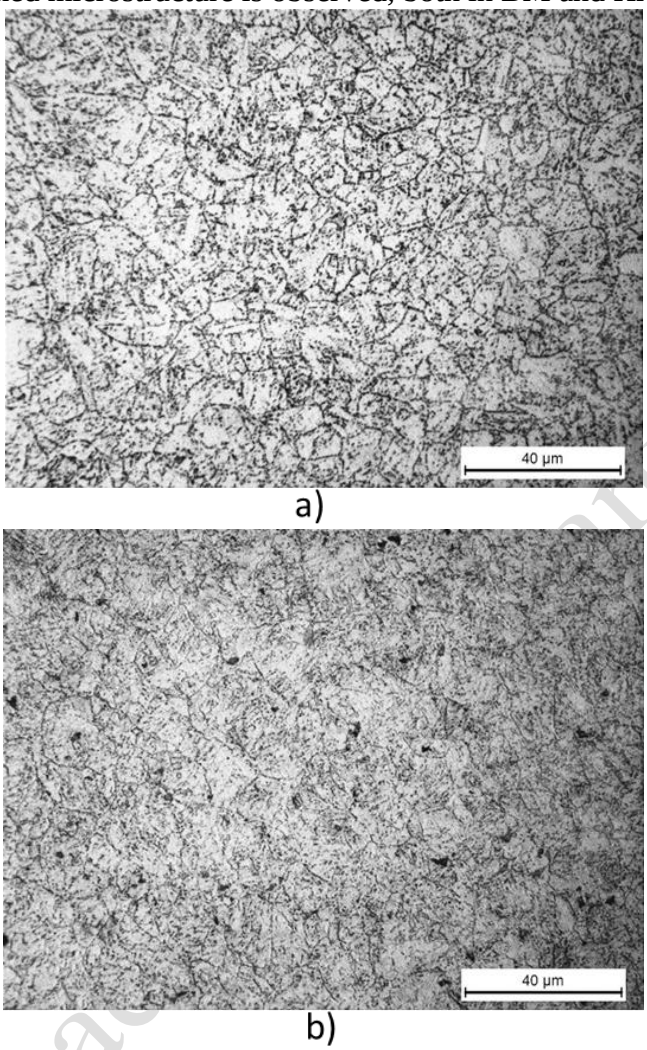

Figure 6. Coarse grained microstructure in: (a) BM and (b) HAZ

Results of hardness measurement are given in Table 3 and shown in Figure 7.

Table 3. Hardness measurements on welded steel SA 387 Gr. 91

Test place	Hardness HV10														
	BM			HAZ			WM			HAZ			BM		
	1	2	3	4	5	6	7	8	9	10	11	12	13	14	15
Zone I	208	208	216	207	206	207	255	241	240	201	209	207	215	212	211
Zone II	209	210	210	214	206	210	256	245	260	207	214	209	207	208	210
Zone III	210	207	209	207	213	215	235	234	225	207	205	209	211	208	210

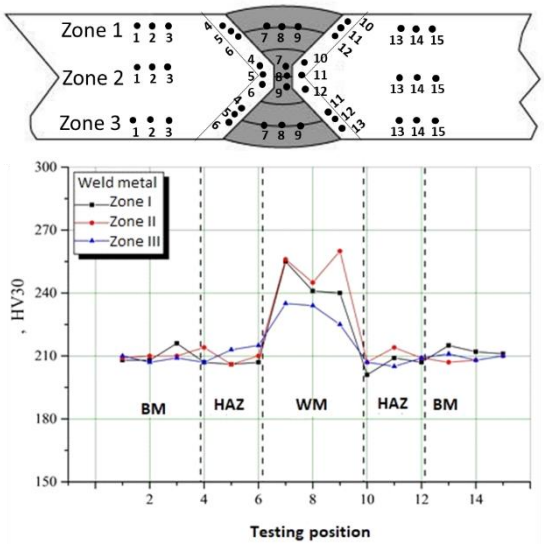

Figure 7. Hardness distribution along the weld

Hardness distribution through the welded joint is symmetrical; the highest values are in the weld metal zone 230-240 HV, while hardness in base metal and heat affected zone have similar values 210 HV with small deviation of measured values for each area.

Typical stress-strain curve obtained in tensile testing of sample welded joint is shown in Figure 8.

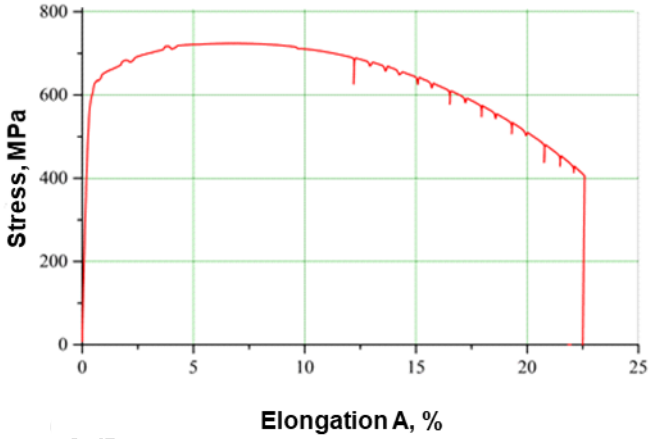

Figure 8. Stress strain curve of welded joint

In elastic part small increase of elongation results in high increase of stress. After reaching apparent yield stress, the rate of increase of slope of σ-ε curve becomes smaller, until reaching Ultimate tensile stress UTS - maximal value, Figure 8. Later, slope is decreasing until moment of fracture. Fracture was always initiated in base metal, while UTS values are 726 MPa. Total elongation before fracture is approximately 22%. Three specimens were tested in order to provide reliability and reproducibility of results. Results obtained in tensile tests are given in Table 4.

Table 4. Results of tensile testing of welded joint

Yield stress, MPa	Ultimate Tensile Stress, MPa	Elongation A, %	Position of fracture
613.2±8	725.9 ±11	21.9±0.8	BM

Bending testing showed no cracks. Detailed results are given in Table 5.

Table 5. Results of bend testing

Sample	Bending angle around face	Sample	Bending angle around root	Grade of radiography

$ZS_L - 1$	180(no cracks)	$ZS_K - 1$	180(no cracks)	2
$ZS_L - 2$	180(no cracks)	$ZS_K - 2$	180(no cracks)	2

Impact testing of weld joint. Three groups of specimens were tested, depending on position V-2 notch, as shown in Figure 9:

- I group - specimens with V-2 notch in base metal (BM),
- II group - specimens with V-2 notch in weld metal (WM)
- III group - specimens with V-2 notch in Heat Affected Zone (HAZ).

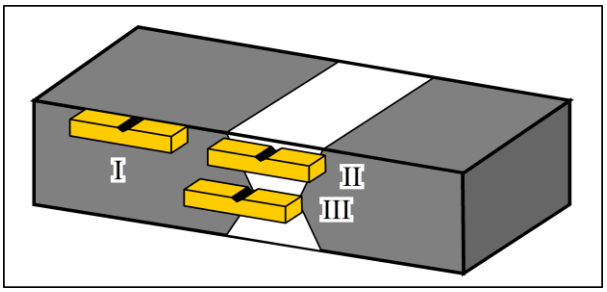

Figure 9. Scheme of Charpy specimen positions in weld joint

Impact testing allowed distinction between crack initiation energy and crack propagation energy. The criterion is obtaining the maximum force in the test, as shown in Figure 10. Energy before maximum force is assigned to crack initiation, while energy after maximum force is assigned to crack propagation [27,28].
Impact testing results for specimens of base metal, weld metal and HAZ are given in Tables 6, 7 and 8, respectively.

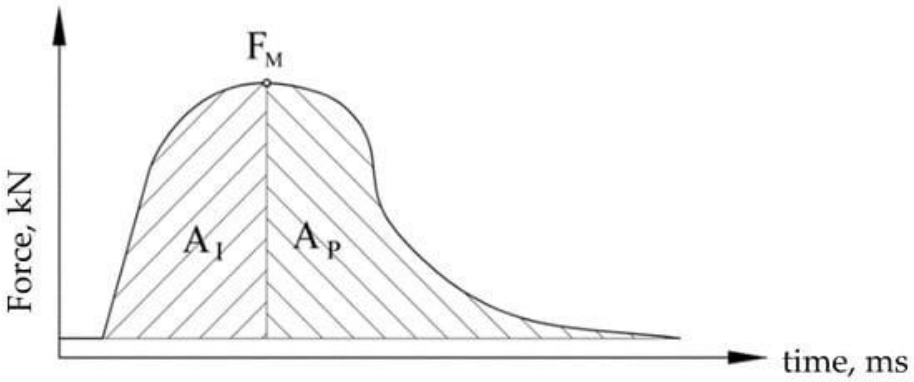

Figure 10. Schematic presentation of evaluation of crack initiation and propagation energies [28]

Table 6. Impact testing of specimen of base metal with V-2 notch

Sample	Total Energy, E_{uk}, J	Energy for crack initiation, E_I, J	Energy for crack propagation, E_P, J
BM 1-1	251	58	193
BM 1-2	268	60	208
BM 1-3	275	55	220
BM 2-1	251	57	194
BM 2-2	271	64	207
BM 2-3	267	60	207

Typical Force-time and energy-time dependences obtained during testing specimens of base metal with notch are shown on Figure 11 (specimen BM-2-1).

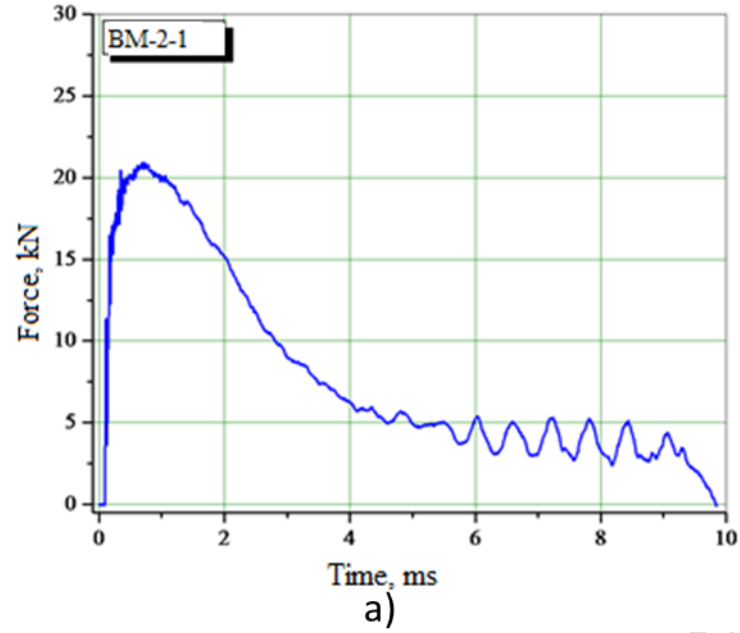

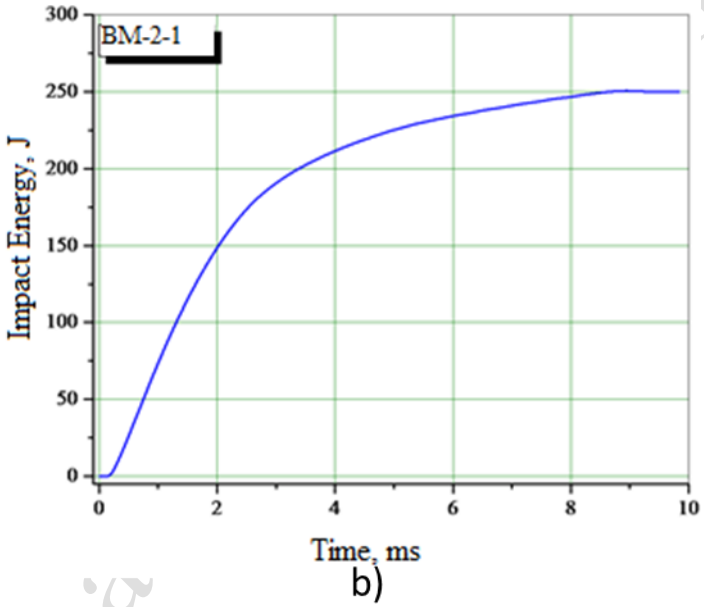

Figure 11. Impact testing of specimen BM-2-1 (base metal)
a) Force-time b) Energy – time

Typical Force-time and energy-time dependences obtained testing specimens of weld metal with notch are shown on Figure 12

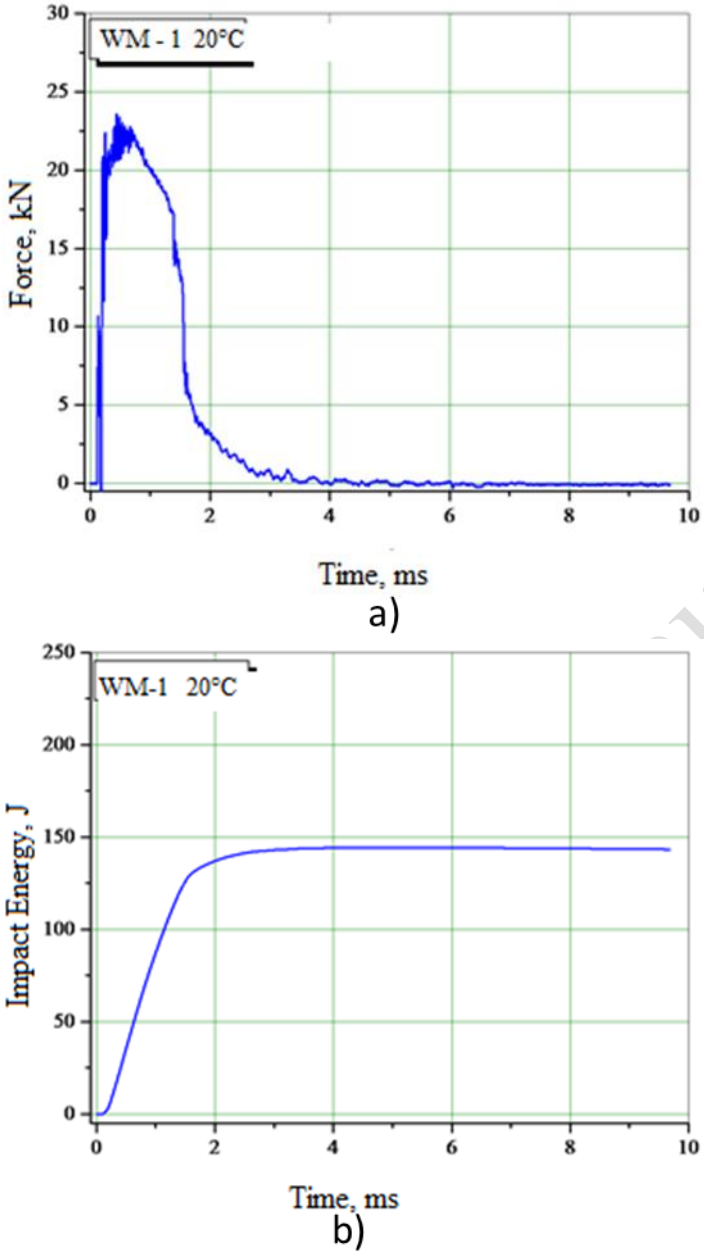

Figure 12. Impact testing of specimen WM-1: (a) Force-time; b) Energy – time.

Table 7. Impact testing of specimen of weld metal with V-2 notch

Sample	Total Energy, E_{uk}, J	Energy for crack initiation, E_I, J	Energy for crack propagation, E_P, J
WM – 1	144	52	92
WM - 2	168	55	113
WM - 3	157	54	103

Typical Force-time and energy-time dependances obtained testing specimens of HAZ with notch (sample HAZ-1) are shown on Figure 13.

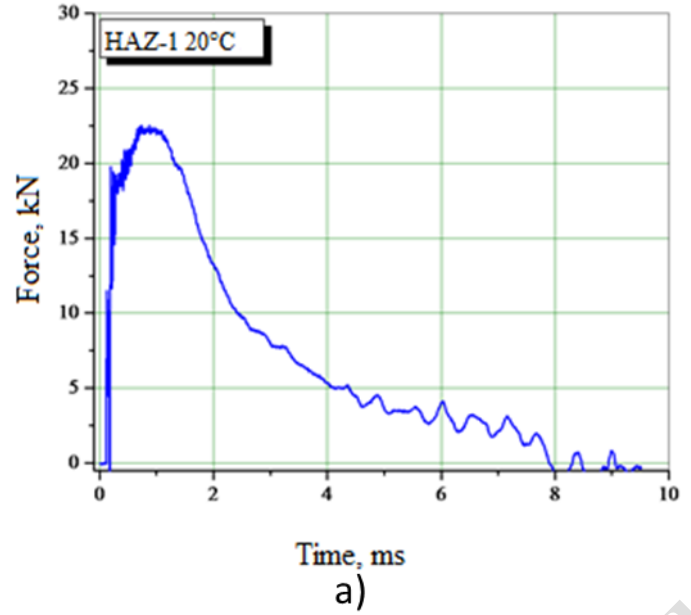

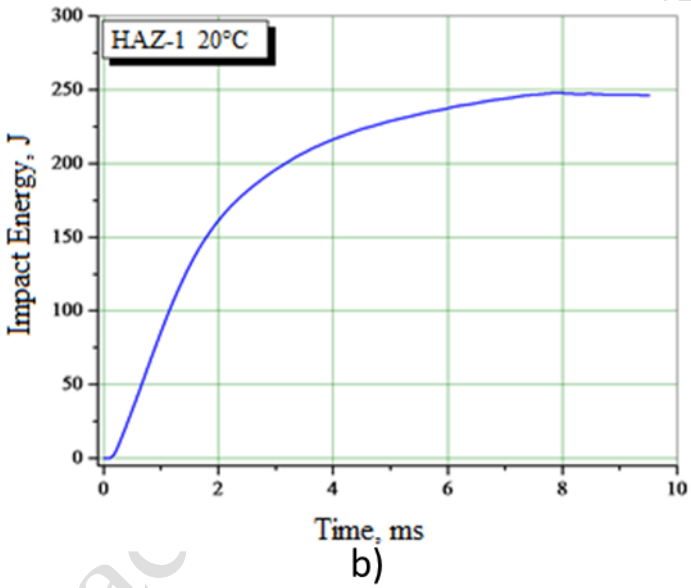

Figure 13. Impact testing of specimen HAZ-1: (a) Force-time; b) Energy – time

Table 8. Impact testing of specimen of HAZ with V-2 notch

Sample	Total Energy, E_{uk}, J	Energy for crack initiation, E_I, J	Energy for crack propagation, E_P, J
HAZ - 1	248	70	178
HAZ - 2	246	59	187
HAZ - 3	249	70	179

Force increases with very high slope, until reaching maximum value, which is followed by decrease. The decrease is strongest in weld metal, while heat affected zone and base metal have similar behavior with smaller decrease.

The total energy for base metal is about 251-267J and the total energy for weld metal is 144-168J, and for heat affected zone 248-249J.

Energies of crack initiation are very similar and they have close values, but of crack propagation shows different values.

The microstructure in simulated sample is in good agreement with microstructures presented on Figures 5 and 6. Measured values of Charpy toughness for simulated sample are given in Table 9.

Table 9. Impact testing of specimen of HAZ with V-2 notch

Sample	Total Energy, E_{uk}, J	Energy for crack initiation, E_I, J	Energy for crack propagation, E_P, J
Simulated HAZ	181,5	121	60,5

DISCUSSION

After quenching, due to intensive cooling during quenching, carbon atoms do not have time to leave austenite and form cementite, so that microstructure consists of martensite (supersaturated ferrite). Depending on alloying, some residual stresses and retained austenite can occur. Martensite is characterized with very high strength and hardness, while toughness is extremely low. In order to improve toughness, reduce retained stresses and eliminate residual austenite, martensite must be tempered [5,9,10,14,15,21].

At the start of tempering, only carbon atoms have sufficient mobility. Therefore, due to diffusion of carbon, precipitation of carbides starts. Since chromium has higher affinity towards carbon than iron, chromium carbides will be nucleated. At this low temperature substitutional solutes do not diffuse [29]. Process intensifies by increase of temperature, when substitutional solutes start to diffuse, enabling intensive nucleation of carbides, not only on grain boundaries, but also within the grains. The final microstructure is characterized with carbides of different size dispersed in a ferritic matrix, showing very small resemblance to the as quenched martensite [5,9,14,15,21].

Obtained microstructure is tempered martensite, Figure 5. Tempered martensite in BM and HAZ is very similar, because both areas have the same chemical composition, as shown in Figures 5a and 5c. On the other hand, some higher content of carbon is responsible for more pronounced carbides in WM, Figure 5b [30].

Hardness measurements confirmed this, because the hardness values in BM and HAZ are similar due to same chemical composition and heat treatment. It is assumed that higher hardness in WM can be attributed to larger presence of carbides [5,9,10,14,15,21] and additional solid solution strengthening due to presence of Ni [5,9,10,14,15].

Apparent yield stress of weld metal (613MPa) is higher than value required for base metal (450MPa). It is worth noting that in all tensile tests, fracture was positioned in base metal, indicating that neither WM nor HAZ are not the critical position [6].

Determination of toughness in HAZ should be approached with high caution. Usual placement of notch in HAZ is based on revealed HAZ on macrostructure, Figure 4. Problem lies in fact that sometimes even initial notch can be placed in different parts of HAZ [26]. Obtained value for energy for crack initiation can be attributed to specific point in microstructure, while crack propagation is never solely in HAZ. This means that energy for crack propagation comprises to certain extent energies for crack propagation in HAZ and BM [26]. Therefore, value of toughness measured in this manner does not reveal fully accurate toughness of microstructure in HAZ. HAZ itself can be divided into subzones depending on peak temperature and subsequent austenitic grain size. Lojen and Vuherer [26] showed relationship between microstructure in different HAZ subzones and impact toughness. In order to overcome this ambiguous situation, it was necessary to prepare sample with microstructure as much as similar to microstructure in HAZ. It was necessary to monitor/register the thermal cycle of HAZ (alternatively this thermal cycle can be calculated based on $t_{8/5}$), and to repeat it on full size Charpy specimen, as shown in Figure 2. Energy for crack initiation in simulated sample is much higher than in welded sample. It can be assumed, that due to several heating cycles (for each welding pass), heat input enabled

increase/growth of carbides in as welded sample, while carbides are smaller in simulated specimen. Smaller carbides provide better toughness, as shown in Tables 6-9. Results of base metal and heat affected zone are in good agreement, because the microstructure in both zones is very similar; values, this is attributed to discrepancy difference in microstructure. In all cases energy for crack initiation is between 55 (WM) and 70 (BM).

The most important difference is in crack propagation. In HAZ, crack propagation energy is approximately 185 J and in weld metal approximately 200 J, while in weld metal is 90-120 J. It is assumed that behavior is due to larger carbides particles. Carbides particles have very sharp edge, what makes them as stress concentrators, so the crack can propagate more easily [31,32] .

It should be noted that even the toughness in weld metal is smallest, it is considerably higher than requirement in standard SRPS EN 10222-2-2017.

For instance, if in a Charpy test piece the area in which the rupture occurs exhibits an inhomogeneous microstructure (like a real weld HAZ does), the energies for the initiation and propagation of the crack and the path of the crack are influenced by all the different microstructures through which the crack propagates. Therefore, the results depend on the microstructure at the bottom of the notch, and on the number and fractions of different types through which the crack propagates. Furthermore, even microstructures in the vicinity of the fracture surface exhibit an influence. It is practically impossible to assure that two test pieces cut from a real weld HAZ would have identical microstructures in the area of rupture. Consequently, the scattering of results is enormous, and the results cannot be linked to only one certain type of microstructure. In order to obtain reliable data on mechanical properties in relation to microstructure, a larger volume of homogeneous microstructure is necessary. On the other hand, simulation can be evaluated as reliable procedure to estimate toughness, since it provides conservative results.

CONCLUSIONS

Steel P91 was welded using combination of GTAW and MMA, for root and filling passes, respectively. Post welding heat treatment consisted of tempering on 740°C for 2h. Since the filler material has similar chemical composition, after final heat treatment microstructure was identified as tempered martensite, in weld metal, heat affected zone and base metal.

- Microstructure in BM and HAZ is very similar, because both areas have the same chemical composition, while, some higher content of carbon is responsible for more pronounced carbides in WM.
- The distribution of hardness revealed slightly higher values in WM. This feature is attributed to slightly higher content of alloying elements introduced by filler material;
- Energy of crack initiation is similar for all three zones. It is assumed that susceptibility for crack initiation of tempered martensite in all zones shows stable value of approx. 60J.
- Energy of crack propagation differs in three zones. In HAZ and BM, crack propagation energy is between 185J and 200J respectively, while in weld metal is 90-120 J. It is assumed that this behavior can be related to presence of larger carbides. Carbides have very sharp edge, what makes them stress concentrators, so the crack can propagate more easily.
- Simulated sample has toughness lower than value recorded from weld butt. It is assumed that, since the presence of HAZ structure in simulated sample covers complete volume, lower toughness is related to coarser carbides. On the other hand, simulation can be evaluated as reliable procedure to estimate toughness, since it provides conservative results.

Acknowledgments

This work was supported by the Ministry of Science, Technological Development and Innovation of the Republic of Serbia (Contract No. 451-03-136/2025-03/200135)". Author Esmail Ali Salem Ahmed appreciates the scholarship from the Ministry of Education of Libya.

Authors contributions

Conceptualization- E.A., T.V., V.G., methodology- T.V., V.G., N.R., experimental validation- D.G., S.D., E.A., writing-original draft preparation- E.A., D.G., T.V.,, writing-reviewing and editing- S.D., N.R., V.G., All authors have read and agreed to the published version of manuscript.

Conflict of intrest

Authors declare no conflict of intrest.

Data availability

Data availability will be provided on request.

Reference

[1] J. Hald, Metallurgy and creep properties of new 9-12%Cr steels, Steel Research 67 (1996) 369–374. https://doi.org/10.1002/srin.199605503.

[2] P.J. Ennis, A. Czyrska-Filemonowicz, Recent advances in creep-resistant steels for power plant applications, Sadhana 28 (2003) 709–730.

[3] B. Arivazhagan, M. Vasudevan, A comparative study on the effect of GTAW processes on the microstructure and mechanical properties of P91 steel weld joints, J Manuf Process 16 (2014) 305–311. https://doi.org/10.1016/j.jmapro.2014.01.003.

[4] D. Poláchová, M. Svobodová, P. Hájková, J. Uzel, Comparision of mechanical properties of P91 steel depending on temperature and annealing time, in: Plzen, 2012.

[5] C. Pandey, M.M. Mahapatra, P. Kumar, N. Saini, Some studies on P91 steel and their weldments, J Alloys Compd 743 (2018) 332–364.https://doi.org/10.1016/j.jallcom.2018.01.120.

[6] B. Arivazhagan, M. Vasudevan, M. Kamaraj, Influence of low nickel (0.09 wt%) content on microstructure and toughness of P91 steel welds, Metals and Materials International 21 (2015) 538–542. https://doi.org/10.1007/s12540-015-4351-8.

[7] C.D. Lundin, Power generation industry materials and their weidability Austenitic stainless steels for nuclear service, Materials &Design 12 (1991) 193–197.

[8] F.V. Ellis, J.F. Henry, B.W. Roberts, Welding, Fabrication, and Service Experience with Modified 9Cr-1Mo Steel, in: Pressure Vessels and Piping of ASME, 1990: pp. 55–63.

[9] Y. Wang, L. LI, Microstructure Evolution of FineGrained HeatAffected Zone in Type IV Failure of P91 Welds, Weld J (2016).

[10] Y. Wang, K.H. Mayer, A. Scholz, C. Berger, H. Chilukuru, K. Durst, W. Blum, Development of new 11%Cr heat resistant ferritic steels with enhanced creep resistance for steam power plants with operating steam temperatures up to 650 °C, Materials Science and Engineering: A 510–511 (2009) 180–184. https://doi.org/10.1016/j.msea.2008.04.116.

[11] C. Coussement, A. Dhooge, E. Van Der Donckt, High Temperature Properties of Improved 9% Cr Steel Weldments, Int. J. Pres. Ves. & Piping 45 (1991) 163–178.

[12] S.H. Babu, G. Amarendra, R. Rajaraman, C.S. Sundar, Microstructural Characterization of ferritic/martensitic steels by positron annihilation spectroscopy, in: J Phys Conf Ser, Institute of Physics Publishing, 2013. https://doi.org/10.1088/1742-6596/443/1/012010.

[13] V. Thomas Paul, S. Saroja, M. Vijayalakshmi, Microstructural stability of modified 9Cr-1Mo steel during long term exposures at elevated temperatures, Journal of Nuclear Materials 378 (2008) 273–281. https://doi.org/10.1016/j.jnucmat.2008.06.033.

[14] S. Kumar, C. Pandey, A. Goyal, A microstructural and mechanical behavior study of heterogeneous P91 welded joint, International Journal of Pressure Vessels and Piping 185 (2020). https://doi.org/10.1016/j.ijpvp.2020.104128.

[15] F.J.G. Silva, A.P. Pinho, A.B. Pereira, O.C. Paiva, Evaluation of welded joints in P91 steel under different heat-treatment conditions, Metals (Basel) 10 (2020). https://doi.org/10.3390/met10010099.

[16] G.C. Bodine, C. Chakravarti, C.M. Owens, B.W. Roberts, D.M. Vandergriff, C.T. Ward, A Program for the Development of Advanced Ferritic Alloys for LMFBR Structural Application, in: ORNL/Sub-4291/1, TR-MCD015, Oak Ridge National Laboratory, 1977.

[17] L. Falat, L. Čiripová, V. Homolová, A. Kroupa, The influence of isothermal ageing and subsequent hydrogen charging at room temperature on local mechanical properties and fracture characteristics of martensitic- bainitic weldments for power engineering, Journal of Mining and Metallurgy, Section B: Metallurgy 53 (2017) 373–382. https://doi.org/10.2298/JMMB170515033F.

[18] H.K.D.H. Bhadeshia, R.W.K. Honeycombe, Steels Microstructure and Properties, ElsevierLtd., 2006.

[19] R.W. Hertzberg, R.P. Vinci, J.L. Hertzberg, Deformation and Fracture Mechanics of Engineering Materials, 6th ed., Wiley, Hoboken, 2020.

[20] E.L. Bergquist, L.E. Svensson, L. Karlsson, Creep Properties of Weldments in Modified 9Cr-1Mo Steel, in: Proceedings of the International Conference on High Temperature Materials, Sigtuna, Sweden, 1998.
[21] C. Pandey, M.M. Mahapatra, Effect of Heat Treatment on Microstructure and Hot Impact Toughness of Various Zones of P91 Welded Pipes, J Mater Eng Perform 25 (2016) 2195–2210. https://doi.org/10.1007/s11665-016-2064-x.
[22] R.W. Swindeman, M.L. Santella, P.J. Maziasz, B.W. Roberts, K. Coleman, Issues in replacing Cr-Mo steels and stainless steels with 9Cr-1Mo-V steel, International Journal of Pressure Vessels and Piping 81 (2004) 507–512. https://doi.org/10.1016/j.ijpvp.2003.12.009.
[23] T.C. Totemeier, J.A. Simpson, H. Tian, Effect of weld intercooling temperature on the structure and impact strength of ferritic-martensitic steels, Materials Science and Engineering: A 426 (2006) 323–331. https://doi.org/10.1016/j.msea.2006.04.023.
[24] C.R. Das, S.K. Albert, A.K. Bhaduri, G. Srinivasan, B.S. Murty, Effect of prior microstructure on microstructure and mechanical properties of modified 9Cr-1Mo steel weld joints, Materials Science and Engineering: A 477 (2008) 185–192. https://doi.org/10.1016/j.msea.2007.05.017.
[25] F. Abe, Torsten-Ulf Kern, Ramaswamy Viswanathan, Creep-resistant steels, Elsevier, 2008.
[26] G. Lojen, T. Vuherer, Optimization of PWHT of simulated haz subzones in p91 steel with respect to hardness and impact toughness, Metals (Basel) 10 (2020) 1–21. https://doi.org/10.3390/met10091215.
[27] R. Prokić-Cvetković, S. Kastelec-Macura, A. Milosavljević, O. Popović, M. Burzić, The effect of shielding gas composition on the toughness and crack growth parameters of AlMg4,5Mn weld metals, Journal of Mining and Metallurgy, Section B: Metallurgy 46 (2010) 193–202. https://doi.org/10.2298/JMMB1002193P.
[28] J.C. Radon, C.E. Turner, Fracture toughness measurements by instrumented impact test*, 1969.
[29] H. Mehrer, The Open-Access Journal for the Basic Principles of Diffusion Theory, Experiment and Application Diffusion in Metals and Intermetallics-an Overview, Basic Principles of Diffusion Theory, Experiment and Application (2022).
[30] M. Taneike, K. Sawada, F. Abe, Effect of Carbon Concentration on Precipitation Behavior of M 23 C 6 Carbides and MX Carbonitrides in Martensitic 9Cr Steel during Heat Treatment, Metallurgical and materials transactions A (2004).
[31] L. Otávio, A. Affonso, Machinery Failure Analysis Handbook: Sustain Your Operations and Maximize Uptime, Gulf Pub, 2006.
[32] M. Svobodová, J. Douda, J. Cmakal, J. Sopoušek, J. Dubskýd, Similar and dissimilar weld joints of creep resisting steels 2009, Hradec nad Moravicí. https://doi.org/10.1016/0013-7944(69)90002-2

List of figures

List of tables